Resonance Raman Spectroscopy and Quantum Chemical Calculations Reveal Structural Changes in the Active Site of Photoactive Yellow Protein†

Masashi Unno,*,‡ Masato Kumauchi,§ Jun Sasaki,§ Fumio Tokunaga,§ and Seigo Yamauchi*,‡

Institute of Multidisciplinary Research for Advanced Materials, Tohoku University, Sendai 980-8577, Japan, and Department of Earth and Space Science, Graduate School of Science, Osaka University, Toyonaka, Osaka 560-0043, Japan

Received January 7, 2002; Revised Manuscript Received February 28, 2002

ABSTRACT: Photoactive yellow protein (PYP) is a bacterial photoreceptor containing a 4-hydroxycinnamyl chromophore. Photoexcitation of PYP triggers a photocycle that involves at least two intermediate states: an early red-shifted PYP_L intermediate and a long-lived blue-shifted PYP_M intermediate. In this study, we have explored the active site structures of these intermediates by resonance Raman spectroscopy. Quantum chemical calculations based on a density functional theory are also performed to simulate the observed spectra. The obtained structure of the chromophore in PYP_L has cis configuration and no hydrogen bond at the carbonyl oxygen. In PYP_M, the cis chromophore is protonated at the phenolic oxygen and forms the hydrogen bond at the carbonyl group. These results allow us to propose structural changes of the chromophore during the photocycle of PYP. The chromophore photoisomerizes from trans to cis configuration by flipping the carbonyl group to form PYP_L with minimal perturbation of the tightly packed protein interior. Subsequent conversion to PYP_M involves protonation on the phenolic oxygen, followed by rotation of the chromophore as a whole. This large motion of the chromophore is potentially correlated with the succeeding global conformational changes in the protein, which ultimately leads to transduction of a biological signal.

A physical understanding of protein structure, dynamics, and function is becoming increasingly important in biology. Since the discovery made by Meyer (*1*), photoactive yellow protein (PYP)[1] has served as an attractive model for such studies. PYP is the 125-residue, 14 kDa cytosolic photoreceptor proposed to mediate negative phototaxis (*2*) in the phototrophic bacterium *Ectothiorhodospira halophila*. This protein has a 4-hydroxycinnamyl chromophore, which is covalently bound to the side chain of Cys69 through a thiolester linkage (*3*, *4*). In a dark state (PYP_{dark}), the chromophore is stablized in the trans configuration as a phenolate anion (*5*, *6*). The phenolate oxygen O1 (see Figure 1 for nomenclature) of the chromophore hydrogen bonds with the hydroxy group of Tyr42 and the protonated carboxyl group of Glu46. In addition, the carbonyl O2 of the chromophore forms a hydrogen bond with the amide group of Cys69 (*5*). Upon photoexcitation of the chromophore, PYP_{dark} enters a photocycle that contains, at least, two intermediate states denoted PYP_L (also called I_1 or pR) and PYP_M (also called I_2 or pB); PYP_{dark} converts to PYP_L in ~3 ns and then to PYP_M with a time constant of ~250 μs. The subsequent recovery of PYP_{dark} by ~350 ms completes the photocycle (*7*, *8*).

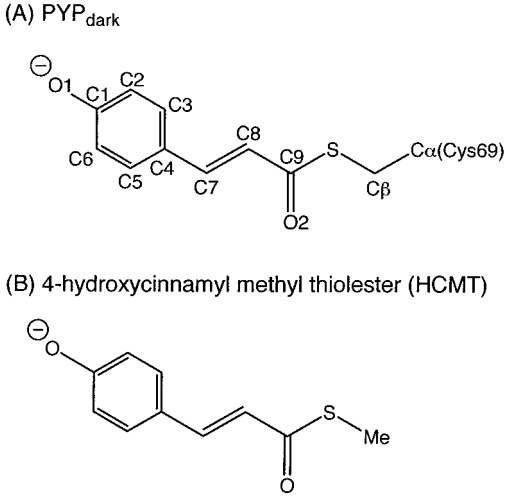

FIGURE 1: (A) Chromophore structure in the dark state. (B) Molecular structure of deprotonated *trans*-4-hydroxycinnamyl methyl thiolester (HCMT).

A mechanism for the photocycle reaction in PYP has been extensively studied, and it is believed that these processes are accompanied by a series of structural changes in the chromophore. The initial photoisomerization of the C7═C8 double bond produces the deprotonated cis chromophore in PYP_L (*9*, *10*), while the transition to PYP_M involves protonation of the phenolic O1 (*4*, *11*). However, it should be emphasized that determination of the chromophore

† This work was supported by grants from the Naito Foundation to M.U. and from the Ministry of Education, Culture, Science, Sports, and Technology to M.U. (10780399) and S.Y. (10044057).

* To whom correspondence should be addressed. Tel: +81-22-217-5618. Fax: +81-22-217-5616. E-mail: unno@tagen.tohoku.ac.jp or yamauchi@tagen.tohoku.ac.jp.

‡ Tohoku University.

§ Osaka University.

[1] Abbreviations: DFT, density functional theory; IR, infrared; HCMT, 4-hydroxycinnamyl methyl thiolester; PYP, photoactive yellow protein; PYP_{dark}, dark-state PYP; PYP_L, red-shifted L intermediate of PYP; PYP_M, blue-shifted M intermediate of PYP; $PYP_{M,dark}$, acid-induced blue-shifted state of PYP.

10.1021/bi025508o CCC: $22.00
Published on Web 04/03/2002

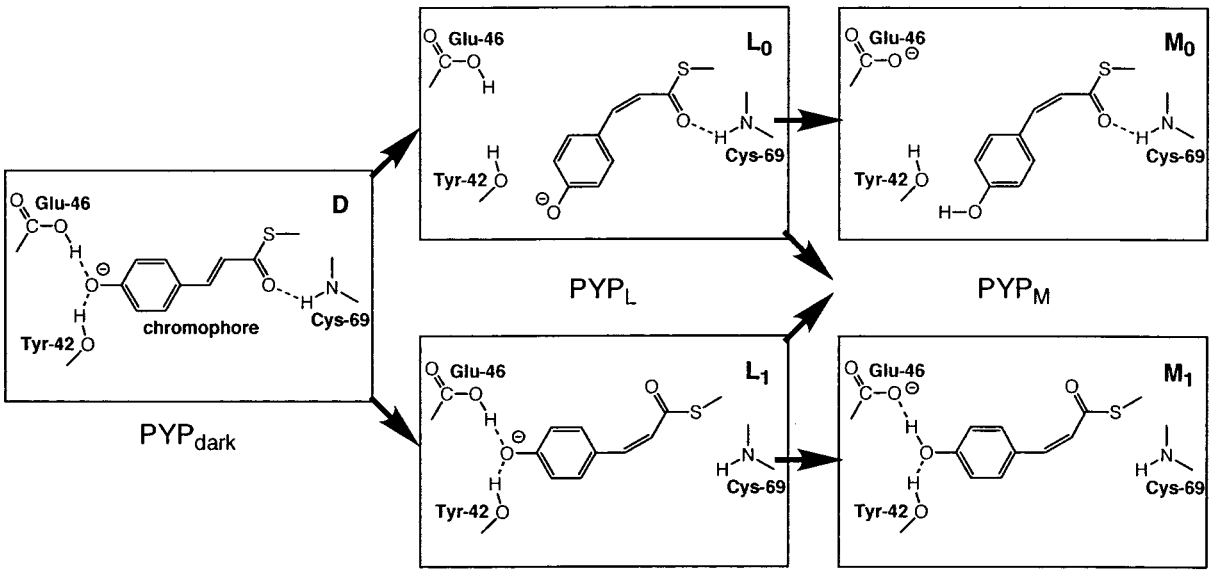

FIGURE 2: Structural model of the PYP photocycle reactions in solution at ambient temperature.

structure for these intermediates is not yet complete in liquid solution at room temperature. For example, the cis configuration for the intermediate states in solutions has been only indirectly demonstrated by a chemical analysis of the chromophore extracted from PYP_M (*12*). In addition, information concerning the chromophore orientation within the protein is still lacking. As illustrated in Figure 2, there are, at least, two possible models for the formation of PYP_L: (i) The first model ($D \rightarrow L_0$) indicates the photoisomerization of the chromophore by rotating the aromatic ring. In this model, a backbone amide hydrogen bonds to the carbonyl O2, whereas the hydrogen bond between Glu46 and the phenolic O1 is broken. (ii) The second model ($D \rightarrow L_1$) involves rotation of the carbonyl group to form a cis chromophore in PYP_L (*13*, *14*), and thereby the carbonyl O2-to-backbone hydrogen bond is disrupted, while the phenolic O1 maintains hydrogen bonds with Tyr42 and Glu46. Crystal structures of PYP_L based on a Laue crystallography (*10*) and a cryotrapped intermediate preceding PYP_L (*9*) supported the latter model. The carbonyl rotation was also suggested for PYP in solution at ambient temperature by time-resolved infrared (IR) spectroscopy (*15*, *16*). The IR studies showed that Glu46 preserves a hydrogen bond supposedly to the phenolic O1 in PYP_L. However, the need for a direct characterization of the chromophore structure is evident.

As in the case of PYP_L, two structural models are conceivable for PYP_M as shown in Figure 2. Both models contain a protonated cis chromophore, where its orientation is different. The models M_0 and M_1 are thus associated with the presence or absence of the hydrogen bond at the carbonyl O2, respectively. The figure further indicates that the simplest mechanism for the PYP_L to PYP_M process comprises protonation of the phenolic O1 without changing the chromophore orientation ($L_0 \rightarrow M_0$ or $L_1 \rightarrow M_1$). It is also possible, however, that in addition to the protonation process the formation of PYP_M involves large movement of the chromophore ($L_0 \rightarrow M_1$ or $L_1 \rightarrow M_0$). Time-resolved Laue crystallographic experiments with 10 ms time resolution (*17*) determined the crystal structure of PYP_M, whose active site structure corresponds to the model M_0 having the carbonyl O2-to-backbone hydrogen bond. However, the structure of PYP_M in the crystal has been challenged by recent spectroscopic (*15*, *16*, *18*−*20*) and theoretical (*21*) investigations, because these studies show larger structural changes in solution than that found in the crystalline state. The contradictory observations suggest that the photocycle in the crystal differs from that in solution. Thus spectroscopic investigations are needed to clarify the active site structures of the intermediate states under physiological conditions.

To explore the photocycle mechanism of PYP in solutions, the presence or absence of the hydrogen bond at the carbonyl O2 as well as the chromophore structure will be key information. Vibrational spectroscopy, such as Raman scattering and IR absorption methods, is ideally suited for this purpose. In general, these techniques are able to provide vibrational frequencies and intensities of individual functional groups with high time resolution. An advantage of Raman spectroscopy over the IR method is its selectivity; i.e., all the protein components contribute to IR spectra, while chromophore and/or protein vibrations can be selected by tuning the laser wavelength in the resonance Raman technique. A resonance Raman spectrum contains further information including protein−chromophore interactions. However, such information has been rarely analyzed because too many structural factors can potentially affect the vibrational frequency. Recently great advances have been made in quantum chemical calculations based on the density functional theory (DFT), with which the Raman spectrum even in larger systems can be simulated without any adjustable parameters. Using both resonance Raman spectroscopy and the DFT calculation, we have now determined the chromophore structure of the intermediate states under physiologically relevant conditions. Moreover, we have successfully extracted information on the carbonyl O2-to-protein hydrogen bond. The results permit us to propose structural models of these intermediates, which reveal the photocycle mechanism of PYP in solutions.

MATERIALS AND METHODS

Preparation of ^{13}C-Labeled Chromophore. ^{13}C-Labeled 4-hydroxycinnamic acid was prepared according to the

Scheme 1: Preparation of ^{13}C-Labeled 4-Hydroxycinnamic Acid[a]

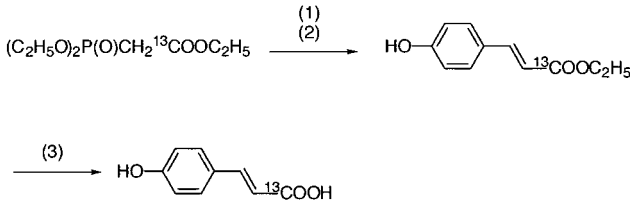

[a] Reagents: (1) sodium hydride in mineral oil (60%) at room temperature under N_2, 30 min; (2) 4-hydroxybenzaldehyde in ether at room temperature under N_2, 2 h; (3) 30% KOH_{aq}, reflux for 2 h.

method described previously (*22*) with minor modification (Scheme 1). The ^{13}C-labeled reagent, triethylphosphonoacetate-$^{13}C_1$ (Aldrich), used was commercially available. Under a nitrogen atmosphere, 4-hydroxybenzaldehyde was treated with the phosphonate anion, which was generated from triethylphosphonoacetate at room temperature. After 4 h of stirring, ethyl 4-hydroxycinnamate was obtained and then hydrolyzed in 30% potassium hydroxide. After the usual workup and purification, colorless 4-hydroxycinnamic acid was obtained. The purity was checked with mass spectrometry and ^{1}H NMR spectroscopy.

Sample Preparation. Production of the wild-type PYP apoprotein by *Escherichia coli*, reconstitution of the holoprotein with the chromophore, and the subsequent protein purification were performed as described previously (*23*). ^{13}C-Labeled PYP was prepared by reconstitution of the apoprotein with the above-mentioned 4-hydroxycinnamic anhydride whose carbonyl carbon atom (C9) was labeled with ^{13}C. PYP in buffered D_2O (90% D_2O/10% H_2O) was prepared by proper dilution of a concentrated protein in 100 mM Tris-HCl buffer at pH 7.4 into D_2O, and then the sample was incubated overnight at room temperature before the measurements.

Resonance Raman Spectroscopy. Resonance Raman spectra were obtained as described earlier (*11*). A liquid nitrogen cooled CCD detector (Instrument S.A., Inc.) recorded the Raman spectra after a Triax190 spectrometer (Instrument S.A., Inc.) removed the excitation light, and a Spex 500M spectrometer (1800 or 3600 grooves/mm grating, 0.5 m focal length) dispersed the scattered light. The 413.1 nm line from a krypton ion laser (BeamLok 2065, Spectra-Physics Lasers, Inc.) or the 325.0 nm line from a helium−cadmium (IK5651R-G, Kimmon Electric Co., Ltd.) laser excited the samples at a 90° angle relative to the axis of the collection optics. A polarization scrambler is placed at the entrance of the spectrometer. All spectra were taken at room temperature (~23 °C), and a homemade software eliminated the noise spikes in the spectra caused by cosmic rays. The measurements for PYP_{dark} and PYP_L were made on samples contained in a quartz spinning cell (10 mm in diameter) or a quartz flow cell (0.3 × 0.3 mm). For the experiments of the spinning cell, a rotation speed of 800 rpm was used, whereas the flow rate was adjusted to 3.3 mL/min for the flow cell measurements. The resonance Raman spectra of PYP_{dark} and PYP_L excited at 413.1 nm were obtained by a single-beam method (*24*), and a transit time of the sample in the beam was ~200 μs. We performed the measurement of PYP_{dark} with a low laser power [0.23 mW; photoalteration parameter (*24*) F = 0.006], while the higher laser power (8.9 mW; F = 2.9) was used for PYP_L. For the measurements of PYP_M, the 441.6 nm line of the helium−cadmium laser was used to produce the intermediate as a photostationary state. The spectra of PYP_M excited at 325.0 nm were obtained using the spinning cell apparatus to minimize the contribution of a species that is photoaltered by the probe light.

DFT Calculation. The optimized geometry, the harmonic vibrational frequencies, and the Raman intensity were calculated using the DFT method via the Gaussian98 program (*25*). The hybrid functional B3LYP and the 6-31G** basis set were used for these calculations. The calculated frequencies were scaled using a factor of 0.9613. Although the experimental spectra were obtained under the resonance condition, the calculated nonresonance Raman intensities realized nicely the obtained spectra in our system: the nonresonance Raman spectra excited at 647.1 nm of PYP_{dark} and an acid-induced bleached state $PYP_{M,dark}$ are very similar to those of their resonance Raman spectra (not shown).

RESULTS AND DISCUSSION

Resonance Raman Spectra and DFT Calculation. Figure 3A depicts resonance Raman spectra of the dark state and two intermediate states of PYP. We measured the resonance Raman spectra of PYP_{dark} with a rapid-flow sampling system comprised of a flow cell and a single laser beam at 413.1 nm. This technique minimizes a contamination of the photoproducts that might build up using stationary cell formats (*24*). The resultant spectrum of PYP_{dark} is consistent with the previous works (*6*, *11*, *26*). The experiments on PYP_L utilized the same rapid-flow apparatus except for a higher incident laser power. By increasing the laser power, the observed spectrum contains signals from a photocycle intermediate in addition to that from PYP_{dark} (*24*). Since a transit time of the sample in the beam was ~200 μs, the photoproduct in the high-power spectrum can be attributed to PYP_L whose lifetime is ~250 μs (*7*, *15*). The lifetimes of the photocycle intermediates preceding PYP_L are shorter than that of PYP_L more than 50-fold (*27*), so that their populations are negligible under the present condition (*24*). Thus, resonance Raman spectra of PYP_L were obtained by subtracting a fraction of the normalized low-power spectrum from the normalized high-power one such that the 1631 cm^{-1} mode of PYP_{dark} disappeared without introducing spurious derivative band shapes or negative peaks. Next we measured the resonance Raman spectrum of PYP_M at 325.0 nm excitation as described previously (*11*). The intermediate PYP_M was produced as a photostationary state by continuous laser illumination at 441.6 nm during the measurement. Because the probe wavelength is only suited for the resonance enhancement of PYP_M (λ_{max} = 355 nm), interference from other species is absent. Note that the measurements of PYP_{dark} and PYP_L were also carried out with a spinning cell, and the observed spectra are nearly the same between the two methods. Because the spinning cell apparatus requires a minimum amount of samples, we performed a series of experiments with the spinning cell and present the data in Figure 3A. It is noted that the figure presents the spectra for PYP_{dark} in D_2O, because some vibrational modes (e.g., ν_{13} and ν_{29}, see below) in H_2O exhibit vibrational coupling (*6*), which complicates the assignment of these modes. In Figure 3A, the resonance Raman spectra are also shown for PYP

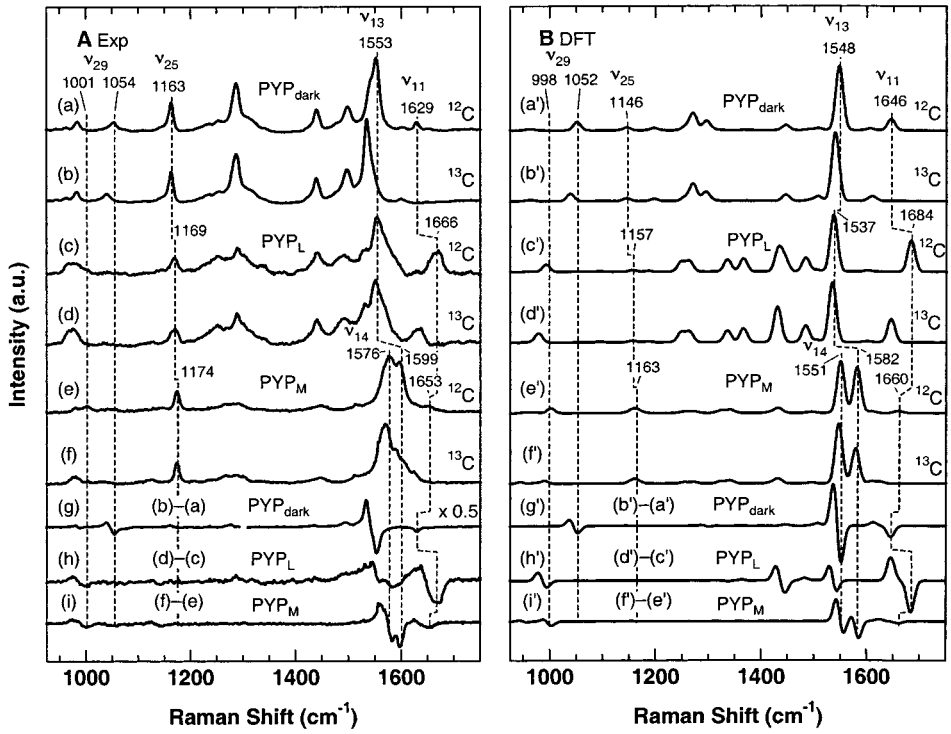

FIGURE 3: Experimentally obtained resonance Raman and simulated Raman spectra of PYP. (A) The following list gives the protein concentration and the buffer condition: PYP_{dark} and PYP_L, 80 μM, 10 mM Tris-HCl buffer, pH 7.4; PYP_M, 100 μM, 10 mM citrate/20 mM phosphate buffer, pH 5.0. For PYP_{dark}, the sample was dissolved in a buffered 90% D_2O/10% H_2O solution. (B) Gaussian band shapes with a 10 cm^{-1} width are used. For PYP_{dark} and PYP_L, intensities for the four highest frequency bands are reduced by a factor of 4 to make lower frequency bands visible in the figure.

whose chromophore is labeled with ^{13}C at the carbonyl carbon atom (C9). The figure further illustrates the $^{12}C/^{13}C$ difference spectra, where the effect of the isotopic substitution can be clearly seen. The data shown in Figure 3A demonstrate that photoconversion of PYP leads to dramatic changes in the spectrum, indicating significant structural alterations in the chromophore and its vicinity. To interpret the experimental results, we have performed DFT calculations as described below.

Among the numerous available DFT methods, we have selected the B3LYP hybrid functional with the 6-31G** basis set because of its high accuracy for predicting vibrational frequencies. It has been shown that this level of DFT calculations yields molecular force fields and vibrational frequencies in excellent agreement with experiments in a variety of systems (*28*). Figure 3B displays the calculated spectra of 4-hydroxycinnamyl methyl thiolester (HCMT; Figure 1), a model of the chromophore. In the present calculation, we introduced intermolecular hydrogen bond(s) around HCMT to mimic the chromophore−protein interaction(s). In the case of PYP_{dark}, we used a deprotonated *trans*-HCMT and placed methanol, acetic acid, and methylamine as a model for Tyr42, Glu46, and the backbone amide of Cys69, respectively. These components were arranged on the basis of the crystal structure of PYP_{dark} (*5*) and subsequently optimized to yield the structure illustrated in Figure 4A. For PYP_L, the starting geometry is based on the crystal structure of the cryotrapped intermediate preceding PYP_L (*9*), where there is no hydrogen bond for the carbonyl O2 in the deprotonated cis chromophore. The structure after optimization is illustrated in Figure 4B. The DFT calculation for PYP_M was also made with a protonated *cis*-HCMT (*11*). Here we have introduced methylamine to mimic the O2-to-backbone hydrogen bond. The starting geometry was taken from a crystal structure of PYP_M (*17*), and the optimized structure is depicted in Figure 4C. Figure 3 demonstrates satisfactory agreements between the experimental and calculated spectra for all species, indicating that the structures shown in Figure 4 give good models for the active site of PYP.

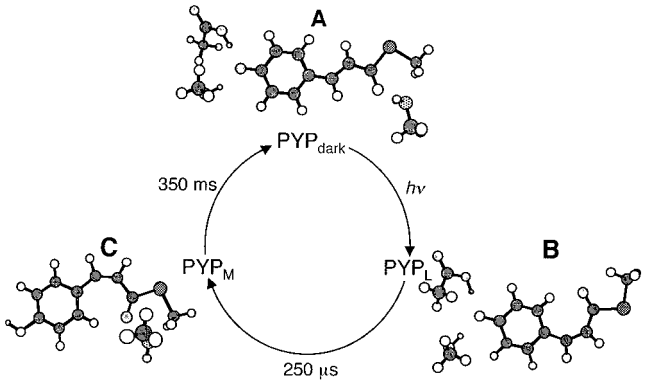

FIGURE 4: Active site structures of PYP. The structures after geometry optimization are displayed for (A) PYP_{dark}, (B) PYP_L, and (C) PYP_M.

Protonation State of Chromophore. We previously showed that the conversion of PYP_{dark} to PYP_M leads to significant changes in the spectrum (*11*). The most remarkable change is an ~30 cm^{-1} upshift of the main band at 1553 cm^{-1} (1558 cm^{-1} in H_2O), and a doublet appears around 1590 cm^{-1}. The band at 1163 cm^{-1} also upshifts by 11 cm^{-1} to 1174 cm^{-1}. As shown in Figure 3B, essentially the same spectral changes are obtained by the DFT calculation. The bands near 1590 cm^{-1} for PYP_M were assigned to coupled C−C and C═C stretching modes of the aromatic ring and vinyl group of

Table 1: Vibrational Frequencies for Some Important Structural Marker Bands

	(A) protonation state markers, ν_{25}, ν_{13}				(B) trans/cis marker, ν_{29}[e]		(C) hydrogen-bonding marker, ν_{11}		
	ν_{25}(obs)/ cm^{-1}	ν_{25}(calc)[a]/ cm^{-1}	ν_{13}(obs)/ cm^{-1}	ν_{13}(calc)[a]/ cm^{-1}	ν_{29}(obs)/ cm^{-1}	ν_{29}(calc)[a]/ cm^{-1}	ν_{11}(obs)/ cm^{-1}	ν_{11}(calc)[c]/cm^{-1}	
								no H-bond	H-bond
PYP_{dark}	1164	1146	1558	1547	1053 (14)[b]	1052 (13)	1631	1671	1643
PYP_L	1169	1157	1553	1537	1001 (15)	993 (14)	1666	1675	1642
PYP_M	1174	1163	1599	1582	1002 (nd)	1002 (14)	1653	1688	1660
$PYP_{M,dark}$	1174[d]		1601[d]		1042[d]		1661[d]	1696	1669

[a] Calculated values. The optimized structures are shown in Figure 4. [b] PYP_{dark} in D_2O buffer. [c] Calculated values for HCMT in the presence or absence of methylamine. The starting geometry was taken from refs *5*, *10*, and *17* for PYP_{dark}, PYP_L, and PYP_M, respectively. For $PYP_{M,dark}$, the starting geometry was obtained by referring to the optimized structure of PYP_{dark}. [d] Reference *11*. [e] The numbers in parentheses are the $^{12}C-^{13}C$ shift in cm^{-1} units. nd = not determined accurately because of the band overlap in ^{13}C-labeled PYP_M.

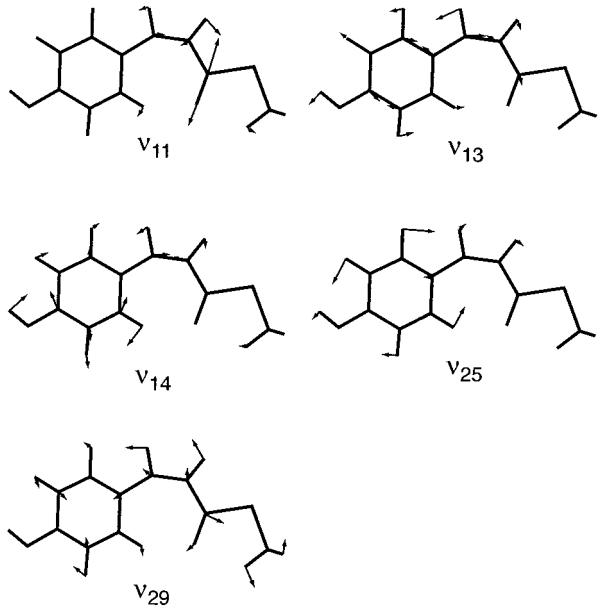

FIGURE 5: Atomic displacement vectors for some vibrational modes of protonated *cis*-4-hydroxycinnamyl methyl thiolester.

the chromophore (*11*). Here we denote the bands at 1576 and 1599 cm^{-1} by ν_{14} and ν_{13}, respectively,[2] whose atomic displacements for these modes are presented in Figure 5. We assign the band near 1170 cm^{-1} as a C−H bending mode ν_{25} for the chromophore aromatic ring (Figure 5), which is analogous to Y9a of tyrosine (*29*). These spectral changes have been ascribed to protonation of the phenolic O1 in PYP_M (*6*, *11*, *16*). In fact, similar spectral alterations were observed upon protonation of a model chromophore (*6*) and upon acid-induced conversion of PYP_{dark} to $PYP_{M,dark}$ (Table 1A) (*11*).

In contrast to PYP_M, the present study has found that the photoconversion of PYP_{dark} to PYP_L leads to relatively small changes in the spectrum (Figure 3A). The bands at 1553 and 1169 cm^{-1} in the spectrum of PYP_L are assigned by the DFT calculation to be ν_{13} and ν_{25}, respectively. The ν_{13} mode is downshifted by 5 cm^{-1} compared to that of PYP_{dark} in H_2O (Table 1A), and the DFT calculation predicts a similar small shift of −10 cm^{-1}. The small downshift for PYP_L contrasts to the case of PYP_M or $PYP_{M,dark}$, where we have found an ∼30 cm^{-1} upward shift. The frequency of ν_{25} in PYP_L (1169 cm^{-1}) is intermediate between those of PYP_{dark} (1164 cm^{-1}) and PYP_M (1174 cm^{-1}), which is also realized by the DFT calculation as 1146, 1157, and 1163 cm^{-1} for PYP_{dark}, PYP_L, and PYP_M, respectively. These results indicate that the chromophore is deprotonated in PYP_L.

Trans/Cis Isomerization of Chromophore. The DFT calculations predict that the frequency of the C8−C9 stretching mode ν_{29} (Figure 5) depends on trans/cis isomerization around the C7═C8 bond. As summarized in Table 1B, deprotonated *trans*-HCMT (PYP_{dark} model) exhibits the ν_{29} band at ∼1050 cm^{-1}, whereas ν_{29} for *cis*-HCMT (PYP_L and PYP_M models) is 990−1000 cm^{-1}, regardless of protonation state of the phenolic O1. The ν_{29} mode can be assigned by the typical isotope shift (ca. −14 cm^{-1}) associated with the ^{13}C substitution of the C9 atom. The experimental resonance Raman spectra shown in Figure 3A exhibit the corresponding downshift (ca. −15 cm^{-1}) upon ^{13}C labeling for the bands at 1054, 1001, and 1002 cm^{-1}, identifying these bands as ν_{29} of PYP_{dark}, PYP_L, and PYP_M, respectively. The ν_{29} mode in both PYP_L and PYP_M downshifts by ∼50 cm^{-1} relative to the frequency in PYP_{dark}, demonstrating a cis configuration chromophore in PYP_L and PYP_M while a trans form in PYP_{dark}. This result indicates that the ν_{29} band is used as a structural marker for trans/cis isomerization of the chromophore.

Chromophore−Protein Hydrogen Bond. To probe the presence or absence of the hydrogen bond at the carbonyl O2 of the chromophore, it is necessary to assign the C9═O2 stretching vibration ν_{11} (Figure 5), because its frequency is expected to be sensitive to hydrogen bonding (*30*). In the previous study (*11*), the highest frequency Raman band of PYP_M at 1653 cm^{-1} has been assigned to the ν_{11} mode. Figure 3A shows that the spectra of PYP_{dark} and PYP_L contain Raman bands at 1629 (1631 cm^{-1} in H_2O) and 1666 cm^{-1}, respectively, that exhibit a large shift (ca. −33 cm^{-1}) due to ^{13}C substitution of C9. We assign these bands as ν_{11}, because the DFT calculation gives rise to these frequencies at 1646 and 1684 cm^{-1} and their $^{12}C/^{13}C$ isotope shifts of −33 and −38 cm^{-1} for PYP_{dark} and PYP_L, respectively (Figure 3). These results indicate that the frequency of the ν_{11} mode significantly varies during the photocycle.

We have carried out further DFT calculations to interpret these dramatic changes in frequency. As a simple model of the active site, we have calculated the vibrational frequency of HCMT in the presence and absence of methylamine, which is a donor of a hydrogen bond for the carbonyl O2. Table 1C shows that formation of the hydrogen bond considerably affects the ν_{11} frequency; i.e., this mode is downshifted by ∼30 cm^{-1} in the presence of methylamine. For PYP_{dark} and PYP_M, a comparison between the observed

[2] A complete assignment of the chromophore vibrations will be presented elsewhere.

and calculated frequencies indicates the presence of the hydrogen bond, since the experimental values of 1631 and 1653 cm^{-1} can be assigned to correspond to those of 1643 and 1660 cm^{-1} in the hydrogen-bonded form, respectively. In contrast, if the calculated frequencies of the PYP_{dark} and PYP_L models are compared, we find that trans to cis isomerization of deprotonated HCMT causes only minor shift of ν_{11} ($-1 \sim +4$ cm^{-1}). Therefore, the experimental result that the ν_{11} mode is upshifted by 35 cm^{-1} on going from PYP_{dark} to PYP_L is only explainable by disruption of the hydrogen bond in PYP_L. This interpretation is consistent with previous studies on the C═O stretching frequency in various systems (*30*, *31*). For instance, Torii et al. (*31*) demonstrated that the C═O stretching frequency of *N*-methylacetamide is upshifted by about 30 cm^{-1} upon removal of a hydrogen bond from the carbonyl oxygen.

The active site structures shown in Figure 4B indicate that the hydrogen bond between the carbonyl O2 and the backbone amide of Cys69 is broken in PYP_L, while the hydrogen bonds from Tyr42 and Glu46 to the phenolic O1 are preserved. The presence of the hydrogen bonds to the phenolic O1 in PYP_L is consistent with recent IR studies on PYP (*15*, *16*), which showed that Glu46 maintains the hydrogen bond presumably to the phenolic O1. The disruption of the hydrogen bond from the carbonyl O2 is also observed in the crystal structures for PYP_L (*10*) and the cryotrapped intermediate proceeding PYP_L (*9*). The structures shown in Figure 4A,B demonstrate that the photocycle of PYP is initiated by flipping the carbonyl group rather than its bulky aromatic ring (D → L_1 in Figure 2). This result implies that the chromophore isomerization requires only minor rearrangements of the chromophore/protein structures during the initial ultrafast events in the photocycle.

In contrast to PYP_L, Figure 4C shows that the carbonyl O2 of the chromophore forms a hydrogen bond in PYP_M. As we have established in this study, both PYP_L and PYP_M have a cis configuration chromophore with deprotonated and protonated phenolic O1, respectively. Thus the presence of the hydrogen bond at the carbonyl O2 in PYP_M suggests that the PYP_L → PYP_M process contains not only the protonation of the O1 but also the rotation of the whole chromophore to re-form the carbonyl O2-to-backbone hydrogen bond (L_1 → M_0). This large movement of the chromophore at a later stage of the photocycle is potentially correlated with the subsequent global conformational changes in the protein (*15*, *16*, *18*−*21*), which lead to the signaling conformation in PYP. Such a large motion of the chromophore may be promoted by formation of a negative charge of Glu46 (*15*).

At this stage, we should comment on another possibility that the carbonyl O2 forms a hydrogen bond with another protein moiety under physiological conditions. Although the hydrogen bond with the amide nitrogen of Cys69 is consistent with the results in the crystalline state (*17*), we cannot completely exclude this idea because of large changes in the protein structure during the formation of PYP_M in solution (*15*, *16*, *18*−*21*). We also comment here on a recent absorption study on mutant PYP (*32*), which suggests the model M_1 for PYP_M. Since the Glu46 → Gln mutation affects the absorption maxima of PYP_L and PYP_M, Glu46 is suggested to interact with the phenolic O1 throughout the photocycle (D → L_1 → M_1). However, this mutation significantly changes the protein structure of PYP_M (*15*), implying that the Glu46 → Gln mutant is not suited to characterize the physiological structure of PYP_M.

CONCLUSION

We have characterized the active site structures of PYP_L and PYP_M by resonance Raman spectroscopy and DFT calculations. On the basis of the determined structures, we have proposed a structural model of the PYP photocycle under physiological conditions. After photon absorption, the chromophore undergoes trans to cis isomerization by flipping the carbonyl group to form PYP_L. Subsequent conversion to PYP_M involves protonation of the phenolic O1, followed by the rotation of the whole chromophore to re-form the carbonyl O2-to-backbone hydrogen bond.

In this study, quantum chemical calculations are effectively used in assigning and interpreting vibrational spectra of PYP photointermediates. We have introduced protein−chromophore interactions in the calculations to obtain detailed structural information that cannot be easily derived from the experiment alone. The current protocol extends the applicability of vibrational spectroscopy to elucidation of dynamic changes in protein−cofactor interactions at an atomic level during the function.

ACKNOWLEDGMENT

We are grateful to N. Hamada (Osaka University) for helpful discussion and to K. Yoshihara (Suntory Institute for Bioorganic Research) for assistance in preparing the ^{13}C-labeled compound.

REFERENCES

1. Meyer, T. E. (1985) *Biochim. Biophys. Acta 806*, 175−183.
2. Sprenger, W. W., Hoff, W. D., Armitage, J. P., and Hellingwerf, K. J. (1993) *J. Bacteriol. 175*, 3096−3104.
3. Hoff, W. D., Düx, P., Hård, K., Devreese, B., Nugteren-Roodzant, I. M., Crielaard, W., Boelens, R., Kaptein, R., Van Beeumen, J., and Hellingwerf, K. J. (1994) *Biochemistry 33*, 13959−13962.
4. Baca, M., Borgstahl, G. E. O., Boissinot, M., Burke, P. M., Williams, D. R., Slater, K. A., and Getzoff, E. D. (1994) *Biochemistry 33*, 14369−14377.
5. Borgstahl, G. E. O., Williams, D. R., and Getzoff, E. D. (1995) *Biochemistry 34*, 6278−6287.
6. Kim, M., Mathies, R. A., Hoff, W. D., and Hellingwerf, K. J. (1995) *Biochemistry 34*, 12669−12672.
7. Hoff, W. D., Stokkum, I. H. M., van Ramesdonk, H. J., van Brederode, M. E., Brouwer, A. M., Fitch, J. C., Meyer, T. E., van Grondelle, R., and Hellingwerf, K. J. (1994) *Biophys. J. 67*, 1691−1705.
8. Meyer, T. E., Yakali, E., Cusanovich, M. A., and Tollin, G. (1987) *Biochemistry 26*, 418−423.
9. Genick, U. K., Soltis, S. M., Kuhn, P., Canestrelli, I. L., and Getzoff, E. D. (1998) *Nature 392*, 206−209.
10. Ren, Z., Perman, B., Srajer, V., Teng, T.-Y., Pradervand, C., Bourgeois, D., Schotte, F., Ursby, T., Kort, R., Wulff, M., and Moffat, K. (2001) *Biochemistry 40*, 13788−13801.
11. Unno, M., Kumauchi, M., Sasaki, J., Tokunaga, F., and Yamauchi, S. (2000) *J. Am. Chem. Soc. 122*, 4233−4234.
12. Kort, R., Vonk, H., Xu, X., Hoff, W. D., Crielaard, W., and Hellingwerf, K. J. (1996) *FEBS Lett. 382*, 73−78.
13. Xie, A., Hoff, W. D., Kroon, A. R., and Hellingwerf, K. J. (1996) *Biochemistry 35*, 14671−14678.
14. Imamoto, Y., Mihara, K., Hisatomi, O., Kataoka, M., Tokunaga, F., Bojkova, N., and Yoshihara, K. (1997) *J. Biol. Chem. 272*, 12905−12908.
15. Xie, A., Kelemen, L., Hendriks, J., White, B. J., Hellingwerf, K. J., and Hoff, W. D. (2001) *Biochemistry 40*, 1510−1517.

16. Brudler, R., Rammelsberg, R., Woo, T. T., Getzoff, E. D., and Gerwert, K. (2001) *Nat. Struct. Biol. 8*, 265−270.
17. Genick, U. K., Borgstahl, G. E. O., Ng, K., Ren, Z., Pradervand, C., Burke, P. M., Srajer, V., Teng, T.-Y., Schildkamp, W., McRee, D. E., Moffat, K., and Getzoff, E. D. (1997) *Science 275*, 1471−1475.
18. Rubinstenn, G., Vuister, G. W., Mulder, F. A. A., Düx, P. E., Boelens, R., Hellingwerf, K. J., and Kaptein, R. (1998) *Nat. Struct. Biol. 5*, 568−570.
19. Kandori, H., Iwata, T., Hendriks, J., Maeda, A., and Hellingwerf, K. J. (2000) *Biochemistry 39*, 7902−7909.
20. Sasaki, J., Kumauchi, M., Hamada, N., Oka, T., and Tokunaga, F. (2002) *Biochemistry 41*, 1915−1922.
21. Shiozawa, M., Yoda, M., Kamiya, N., Asakawa, N., Higo, J., Inoue, Y., and Sakurai, M. (2001) *J. Am. Chem. Soc. 123*, 7445−7446.
22. William, S. W., Jr., and William, D. E. (1961) *J. Am. Chem. Soc. 83*, 1733−1738.
23. Imamoto, Y., Ito, T., Kataoka, M., and Tokunaga, F. (1995) *FEBS Lett. 374*, 157−160.
24. Mathies, R. A., Smith, S. O., and Palings, I. (1988) in *Biological Applications of Raman Spectroscopy* (Spiro, T. G., Ed.) Vol. II, pp 59−108, Wiley-Interscience, New York.
25. Frisch, M. J., Trucks, G. W., Schlegel, H. B., Scuseria, G. E., Robb, M. A., Cheeseman, J. R., Zakrzewski, V. G., Montgomery, Jr., J. A., Stratmann, R. E., Burant, J. C., Dapprich, S., Millam, J. M., Daniels, A. D., Kudin, K. N., Strain, M. C., Farkas, O., Tomasi, J., Barone, V., Cossi, M., Cammi, R., Mennucci, B., Pomelli, C., Adamo, C., Clifford, S., Ochterski, J., Petersson, G. A., Ayala, P. Y., Cui, Q., Morokuma, K., Malick, D. K., Rabuck, A. D., Raghavachari, K., Foresman, J. B., Cioslowski, J., Ortiz, J. V., Baboul, A. G., Stefanov, B. B., Liu, G., Liashenko, A., Piskorz, P., Komaromi, I., Gomperts, R., Martin, R. L., Fox, D. J., Keith, T., Al-Laham, M. A., Peng, C. Y., Nanayakkara, A., Gonzalez, C., Challacombe, M., Gill, P. M. W., Johnson, B., Chen, W., Wong, M. W., Andres, J. L., Gonzalez, C., Head-Gordon, M., Replogle, E. S., and Pople, J. A. (1998) *Gaussian98*, Gaussian, Inc., Pittsburgh, PA.
26. Zhou, Y., Ujj, L., Meyer, T. E., Cusanovich, M. A., and Atkinson, G. H. (2001) *J. Phys. Chem. A 105*, 5719−5726.
27. Ujj, L., Devanathan, S., Meyer, T. E., Cusanovich, M. A., Tollin, G., and Atkinson, G. H. (1988) *Biophys. J. 75*, 406−412.
28. Koch, W., and Holthausen, M. C. (2000) *A Chemist's Guide to Density Functional Theory*, Wiley-VCH, Weinheim.
29. Harada, I., and Takeuchi, H. (1986) in *Spectroscopy of Biological Systems* (Clark, R. J. H., and Hester, R. E., Eds.) Vol. 13, Chapter 3, John Wiley & Sons, Chichester.
30. Tonge, P. J., and Carey, P. R. (1992) *Biochemistry 31*, 9122−9125.
31. Torii, H., Tatsumi, T., and Tasumi, M. (1998) *J. Raman Spectrosc. 29*, 537−546.
32. Imamoto, Y., Mihara, K., Tokunaga, F., and Kataoka, M. (2001) *Biochemistry 40*, 14336−14343.

BI025508O